Polymer Chemistry

ROYAL SOCIETY OF CHEMISTRY

PAPER

View Article Online
View Journal | View Issue

Cite this: *Polym. Chem.*, 2025, **16**, 589

Photobase-catalyzed thiol–ene click chemistry for light-based additive manufacturing†

J. Antonio Vazquez, [a] Xabier Lopez de Pariza,[b] Nathan Ballinger,[a] Naroa Sadaba,[a] Aileen Y. Sun,[c,d] Ayokunle O. Olanrewaju, [c,d] Haritz Sardon [b] and Alshakim Nelson *[a]

Photo-mediated additive manufacturing from liquid resins (vat photopolymerization) is a rapidly growing field that will enable a new generation of electronic devices, sensors, and soft robotics. Radical-based polymerization remains the standard for photo-curing resins during the printing process due to its fast polymerization kinetics and the range of available photoinitiators. Comparatively, there are fewer examples of non-radical chemical reactions for vat photopolymerization, despite the potential for expanding the range of functional materials and devices. Herein, we demonstrate ionic liquid resins for vat photopolymerization that utilize photo-base generators (PBGs) to catalyze thiol-Michael additions as the network forming reaction. The ionic liquid increased the rate of curing, while also introducing ionic conductivity to the printed structures. Among the PBGs explored, 2-(2-nitrophenyl)-propyloxycarbonyl tetramethylguanidine (NPPOC-TMG) was the most effective for the vat photopolymerization process wherein 250 μm features were successfully printed. Lastly, we compared the mechanical properties of the PBG catalyzed thiol-Michael network *versus* the radical polymerized network. Interestingly, the thiol-Michael network had an overall improvement in ductility compared to the radical initiated resin, since step-growth methodologies afford more defined networks than chain growth. These ionic liquid resins for thiol-Michael additions expand the chemistries available for vat photopolymerization and present opportunities for fabricating devices such as sensors.

Received 6th October 2024,
Accepted 20th December 2024

DOI: 10.1039/d4py01120a

rsc.li/polymers

1. Introduction

Additive manufacturing, or 3D printing, is a rapidly growing field that will enable the fabrication of devices, sensors, and soft robots for industries such as aerospace and medicine.[1] In photo-mediated additive manufacturing from liquid resins (vat photopolymerization), polymerizable layers of resin are cured in a sequential manner to produce a 3D construct. While advances in printing technologies have vastly improved the resolution and speed of vat photopolymerization,[2–4] the chemical reactions for network formation have primarily focused on free-radical polymerization of acrylates and methacrylates.[5] Photo-generated radicals can also be used in thiol–ene reactions to create polymer networks *via* step-growth polymerization.[6–8] Alternate chemistries for network formation will be pivotal as the field moves towards multiwavelength printing, allowing the incorporation of diverse functionalities into additive manufacturing.[9,10]

Photobase generators (PBG) can expand the chemical reactions available for vat photopolymerization to enable recyclability, degradability, and compatibility with radical-sensitive additives.[11–14] PBGs are molecules that release organic bases upon light irradiation. Base-catalyzed thiol-click chemistry is a viable strategy for vat photopolymerization because the reactions are rapid, selective, and achieve high degree of conversion.[15–19] For example, Lopez de Pariza and coworkers demonstrated the first example of a base-catalyzed resin for digital light processing (DLP) 3D printing using a photolabile guanidinium salt and thiol-isocyanate addition as the network forming reaction.[20] The resulting poly(thiourethane) was self-healing and recyclable due to the thiol-isocyanate dynamic bonds. More recently, the Page group has expanded the use of PBGs in vat photopolymerization of thiol-isocyanate resins by synthesizing a series of new PBGs for vat photopolymerization.[21] The Page group also developed a dual-curing resin for a thiol-acrylate resin using a PBG in combination

[a]*Department of Chemistry, University of Washington, Seattle, WA 98195, USA. E-mail: alshakim@uw.edu*
[b]*POLYMAT and Department of Polymers and Advanced Materials: Physics, Chemistry and Technology, Faculty of Chemistry, University of the Basque Country UPV/EHU, Donostia-San Sebastián 20018, Spain. E-mail: haritz.sardon@ehu.es*
[c]*Department of Bioengineering, University of Washington, Seattle, WA 98195, USA*
[d]*Department of Mechanical Engineering, University of Washington, Seattle, WA 98195, USA. E-mail: ayokunle@uw.edu*

† Electronic supplementary information (ESI) available. See DOI: https://doi.org/10.1039/d4py01120a

with a photoradical generator to allow for the printing of constructs with a wide range of moduli depending on the mechanism of curing.[22] PBGs have also been shown to polymerize a thiol-acrylate resin in a two-photon polymerization system. The authors observed that this approach resulted in materials with a more homogenous network relative to the uncontrolled morphology of chain-growth polymerized networks.[23] There have been significant strides on the incorporation of PBGs into photosensitive resins increasing the resin diversity for vat photopolymerization.

Vat photopolymerization of ionic liquids enables the printing of functional materials which are ionically conductive with diverse applications as sensors, solid polymer electrolytes, and shape morphing constructs.[24–29] Ionic liquids (IL) are room temperature salts and they stand out as a desirable alternative to conventional solvents due to their negligible vapor pressure, good thermal stability, and ionic conductivity.[30] Moreover, the broad design space of ILs can be leveraged to better dissolve additives, tune the viscosity of a resin, or serve as a reactive diluent. Introducing PBGs into an ionic liquid resin could broaden the applicability of these vat photopolymerization catalysts.

Herein, we demonstrate ionic liquid resins for vat photopolymerization that utilize photo-base generators (PBGs) to catalyze thiol-Michael additions as the network forming reaction. The resin was composed of poly(ethylene glycol)diacrylate (PEGDA), trimethylolpropane tris(3-mercaptopropionate) (TMPTMP), 1-ethyl-3-butylimidazole bistriflimide ([EBIM] TFSI), and 2-(2-nitrophenyl)-propyloxycarbonyl tetramethylguanidine (NPPOC-TMG) as the photobase generator (Fig. 1b). The ionic liquid was necessary to formulate a fast curing resin with appropriate viscosity (below 10 Pa s)[31] and shown to be printable on a commercially available printer. The optimal resin composition, characterized by low viscosity and rapid photo-induced gelation, was determined using rheology. Additionally, we compared the performance of PBG *versus* a photoradical generator in the formation of polymer networks.

2. Results and discussion

In this study we utilized PBGs to create a resin that is photocurable *via* a base-catalyzed pathway with PEGDA and TMPTMP as the monomers and ionic liquid to formulate a DLP printable ionogel (Fig. 1). The network forming reaction that we expect is a thiol-Michael addition (Fig. 1a), making this a step-growth polymerization mechanism. Ionic liquids were chosen for the ability to tune the solvents properties and provide ionic conductivity.[30]

To prepare the photocurable resin, the Michael acceptor monomer, PEGDA, and PBG were dissolved in ionic liquid, and the trithiol monomer (TMPTMP) was added immediately before conducting the experiment. A stoichiometric balance between the thiol [SH] and acrylate [C=C] functional groups was targeted with each resin preparation due to the step growth nature of the polymerization. Four imidazolium ionic liquids, 1-butyl-3-vinyl imidazolium [BVIM] TFSI, 1-butyl-3-methyl imidazolium [BMIM] TFSI, [BVIM] tetrafluoroborate (BF_4), and [EBIM] TFSI; and two photobase generators, 1,8-diazabicyclo(5.4.0)undec-7-ene tetraphenylborate (DBU·$HBPh_4$) and NPPOC-TMG were tested. Synthetic procedures and characterization data of the ILs and PBGs can be found in the ESI (Fig. S1–5†). Photocuring experiments were performed on a rheometer equipped with 365 nm light at an intensity of 20 mW cm^{-2}. Photocuring of resins formulated with DBU·$HBPh_4$ were used to select the best ionic liquid by comparing the relative gel points. We found that [EBIM] TFSI resulted in a gel point of 37 s with [BVIM] TFSI following at 67

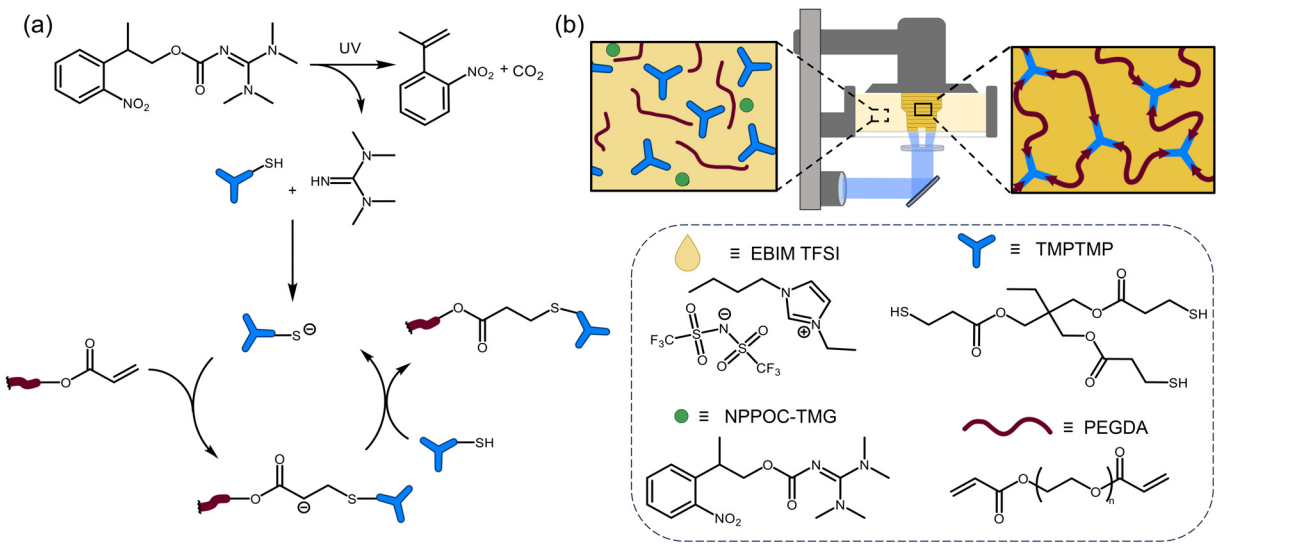

Fig. 1 Base-catalyzed thiol-Michael DLP printing (a) reaction mechanism for photolysis of PBG and thiol-Michael reaction, (b) cartoon of DLP printer and chemical structures of resin components.

s (Fig. S6a†), so [EBIM] TFSI was selected for further experiments. The faster gel point for [EBIM] TFSI was due to better solubility of the PBG in this ionic liquid. We found that a minimum of 25 wt% IL was necessary to dissolve the PBG with [EBIM] TFSI giving the clearest solution. We then compared the PBGs using [EBIM] TFSI and found that NPPOC-TMG resulted in slightly faster gelation (30 s) (Fig. S6b†) without requiring isopropylthioxanthone (ITX) which would homopolymerize the acrylates (green trace in Fig. S6b†). For comparison, NPPOC-TMG was also dissolved in neat monomers without the ionic liquid; however, photocuring of the resin was much slower and required 80 s to reach gel point (Fig. S6c†). Solvent polarity has been shown to influence thiol-Michael reaction kinetics, which could lead to the observed difference in curing rates.[32] Based on the photocuring experiments the optimal ionic liquid and PBG were [EBIM] TFSI and NPPOC-TMG, respectively.

The resin with optimal components was characterized to meet three key criteria: (1) rapid curing at 385 nm, (2) stability in the dark, and (3) low viscosity for effective recoating.[33] Rheological experiments can assess these characteristics to select the best resin composition for vat photopolymerization by comparing the crossover point of the storage modulus over the loss modulus, or the gel point. Photocuring experiments showed that NPPOC-TMG could cause gelation of the step-growth thiol-Michael network within 30 s at 1 wt% (Fig. 2a). The resin with 2 wt% NPPOC-TMG had a gel point at 23 s, while reducing the NPPOC-TMG to 0.5 wt% in a gel point 42 s. In addition to fast UV curing, a photocurable resin should not exhibit a large change in the storage modulus until it is irradiated. Therefore, the stability of the resin in the dark was investigated by performing a time sweep (Fig. 2b) at a constant strain amplitude (5 Pa). The time sweep experiments indicated that the resin is stable for 3 hours, which is the maximum amount of time required to print a structure using this formulation. The loss modulus must be greater than the storage modulus for a resin intended for DLP printing, which is indicative of a material with a dominant liquid-like character.[33] The resin maintains this behavior throughout the 3 hours with no crossover of the loss and storage moduli pro-

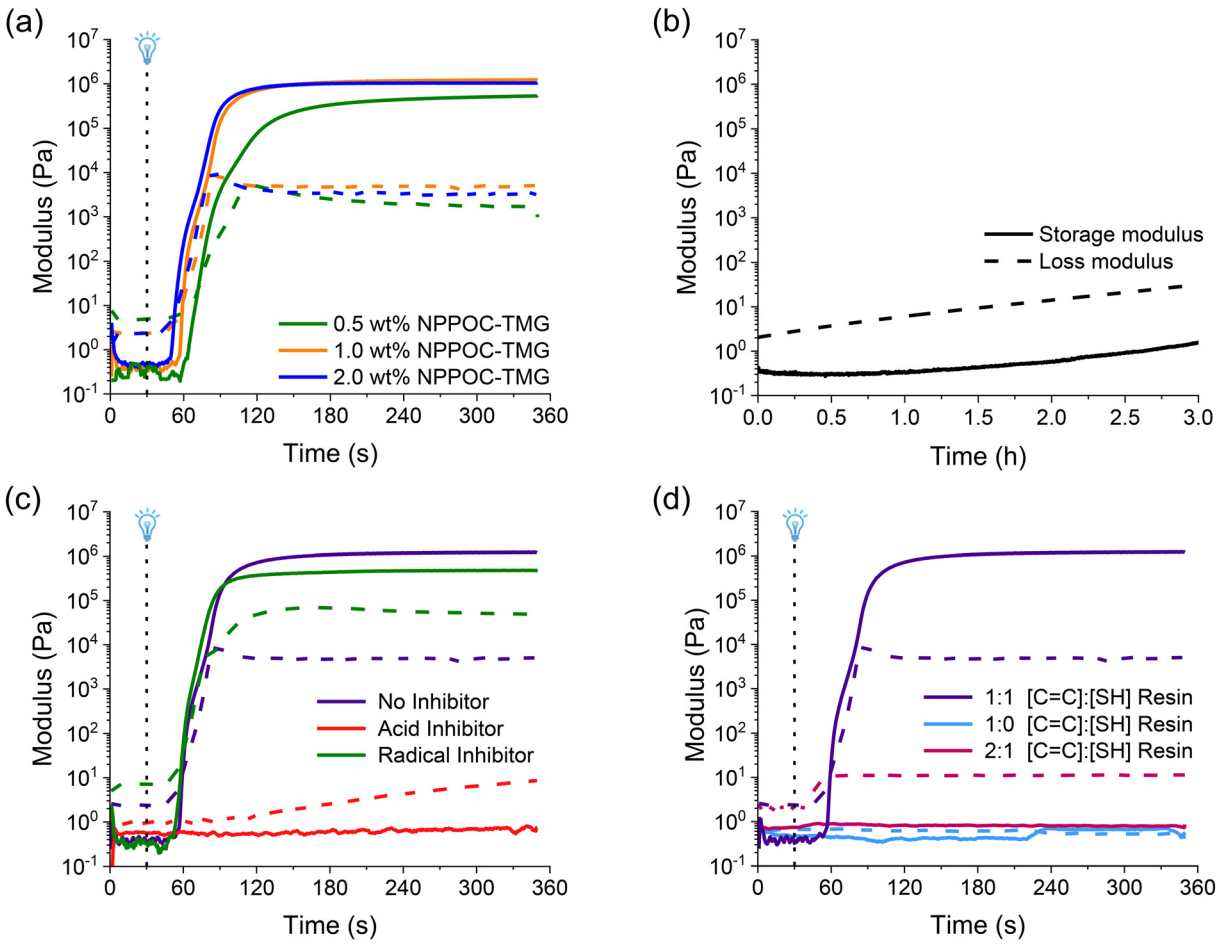

Fig. 2 Rheology of thiol-Michael resins; dashed lines are G'' and solid lines are G'. Rheological conditions for photorheology: 1 Hz, 1% strain, light on at 30 s. (a) UV curing experiment showing the effect of NPPOC-TMG concentration. (b) Dark stability of the resin (5 Pa strain amplitude, no light, 3 h). (c) UV curing of resins with radical inhibitor or organic acid. (d) UV curing comparing resins without trithiol monomer and substoichiometric thiol content.

viding sufficient time to print. Lastly, our rheological experiments (Fig. S18†) showed that the IL increased the viscosity of the resin slightly, but remained below 1 Pa s.

In addition to exploring the optimal printing conditions, rheological experiments were performed to ensure that there was no homopolymerization of the acrylates by radical formation, and that the reaction proceeds *via* a base-catalyzed thiol-Michael mechanism. First, we added TEMPO as a radical inhibitor to the resin formulation as this would impede any radical mediated reactions occurring in the resin that could lead to acrylate homopolymerization.[34] In order to show that generation of the base was critical for the network forming reaction, we added octanoic acid as a scavenger acid to the resin formulation. The octanoic acid would be preferentially deprotonated therefore no thiolate would form resulting in no network formation. The resins were prepared with an equimolar amount of inhibitor to the NPPOC-TMG to ensure full inhibition if needed. The rheological experiments showed that TEMPO (green trace in Fig. 2c) had no significant effect on the curing rate of the resin indicative that radicals are not responsible for network formation. In contrast, with the addition of equimolar quantity of octanoic acid (red trace in Fig. 2c) there is no gel point and only a slight increase in the loss modulus. These results demonstrate that thiolate anions are required for crosslinking. Next, to further demonstrate the dependency on trithiol monomer, resin formulations with no thiol and substoichiometric concentration of thiols were investigated (Fig. 2d). In the absence of trithiol monomer (blue trace in Fig. 2d), there was no gelation even after 5 min of irradiation providing evidence for little to no crosslinking which suggests that little to no radical generation occurs during the PBG activation which correlates well with previously published studies for UV curing with NPPOC-TMG.[17] In contrast, a resin made with a substoichiometric amount of trithiol monomer (pink trace in Fig. 2d) produced a rapid increase in the loss modulus demonstrating the requirement for the trithiol crosslinker to form a polymer network *via* a thiol-Michael mechanism. These experiments suggest that homopolymerization of acrylates is minimal, and that rapid network formation is dependent on the presence of the trithiol monomer.

We next demonstrated the printability of these resins with a commercial DLP printer (Asiga Freeform Max-UV) equipped with a 385 nm light source at an intensity of 20 mW cm^{-2}. The photonic parameters of the resin were obtained using a Jacobs working curve (eqn (1)):

$$C_d = D_p \ln E_0 - D_p \ln E_c \quad (1)$$

where C_d is the depth or thickness of the cured resin, E_0 is the radiant exposure dose on the surface of the resin, E_c is the "critical" energy required to reach the gel point of the resin, and D_p is the penetration depth of the light into the resin.[35] The working curve was obtained by following two methods, a typical method using a spot timer on the printer and digital calipers (Fig. 3a) and a method which utilized a rheometer outlined by Rau *et al.*, (Fig. S8†).[36] From the working curve, the exposure

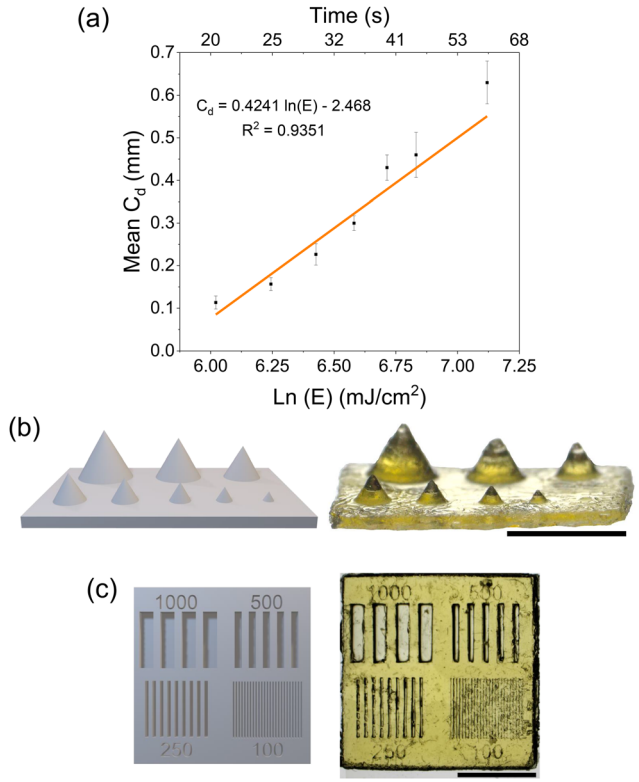

Fig. 3 Jacobs working curves of the PBG resin and printed objects used to investigate print fidelity. (a) Working curve obtained from the Asiga printer. (b) Cones of varying radii (from far-left corner radii were 1.5, 1.25, 1.0, 0.75, 0.625, 0.5, 0.375, and 0.25 mm) on a rectangular plate, (c) optimization chip with channels (areas where resin was uncured) and features (lines between channels that were cured) that were 1000, 500, 250 and 100 μm in width and 0.6 mm in depth. Scale bars are all 5 mm scale.

time (t_c) required to reach the critical energy of a specific thickness can be determined. We aimed to print 50 μm layers, so the working curve obtained with the rheometer resulted in t_c = 15.4 s. To compare how the light source on the printer affects the curing an additional working curve was generated. The working curve obtained with the light source from the printer resulted in a t_c = 18.4 s which was slightly longer exposure time than the prediction with the rheometer. As shown in Fig. S9,† NPPOC-TMG has a higher absorbance at 365 nm than 385 nm causing the difference in t_c values obtained from the rheometer *versus* the working curves. The rheometer is equipped with a 365 nm light source and the printer has a 385 nm light source, so we decided to use the working curve obtained with the printer. To ensure good interlayer adhesion, exposure times of 1.2–2 times greater than the critical exposure time is typically necessary. Therefore, we began printing with 22 s layer times. Printing optimization structures (Fig. 3b and 3c) the optimized exposure time was found to be 30 s per layer which provided structures with decent resolution.

Next, we looked at the print fidelity of the 3D printed array of cones and the array of channels. The array of cones showed that the resin could resolve positive features down to 375 μm

(Fig. 3b) while the optimization chip resolved features and channels down to 250 μm (Fig. 3c). Closer inspection of the printed parts was carried out by optical profilometry using a Keyence VHX-970 digital microscope to analyze the dimensional accuracy of the microfeatures (Fig. S16 and S17†). The images collected were then analyzed using ImageJ software to measure the width at half height of the channels and features of the optimization chip which were summarized in Table 1.

Overall, the channels were smaller than expected due to overcuring, resulting in the features (lines between channels) being larger than expected. Nevertheless, the resin was capable of curing features and channels lines down to 250 μm resolution with the channels being on average 64% smaller and the features 130% larger. The resin was unable to reliably print features or channels at 100 μm. These conditions were used to print more complex shapes (Fig. S15†) with good resolution. The Asiga UV MAX X printer has a pixel resolution of 43 μm which was smaller than the resolution achieved in the prints. The limitation caused by the chemistry was attributed to (i) the low light absorption of NPPOC-TMG at 385 nm requiring long exposure times, and (ii) the high optical transparency of the resin that led to deep light penetration and overcuring. The print fidelity could be improved in the future by modification of the photobase generator or with the inclusion of a photoabsorber.[37] 3D-printing parameters including exposure time, light intensity, layer height, and lift and retract speed can also be optimized to improve feature resolution and print reproducibility.[38]

Next, we compared the mechanical properties of radical-mediated networks against base-catalyzed networks. Thiol-acrylate systems that use radical initiators can react *via* a combination of step-growth (to afford thiol–ene adducts) and chain-growth polymerizations (to afford polyacrylates).[18,39–41] In contrast, base-catalyzed reactions between thiols and acrylates produced a network derived only from step-growth polymerization. Thus, we formulated a resin with phenylbis (2,4,6-trimethylbenzoyl) phosphineoxide (BAPO) as a radical initiator in exchange for the PBG. The resins were compared by casting dogbones for tensile experiments which were cured using a 385 nm light source with an intensity of 20 mW cm^{-2}. The BAPO initiated resin resulted in ionogels (Fig. 4a) with an average Young's modulus of 1466.5 ± 191.9 kPa and average strain at break of 29.655% ± 8.135. While the NPPOC-TMG initiated ionogels had an average Young's modulus of 616.13 ± 57.49 kPa and average strain at break of 76.185 ± 17.909% (Table S1†). Overall, the radical-initiated samples had higher tensile moduli and exhibited failure at smaller strains. In comparison, the printed dogbones had comparable mechanical properties to the casted dogbones when radically initiated (Fig. 4b), while the base-catalyzed resin printed dogbones had slightly improved mechanical properties (Fig. 4c).

The difference in mechanical properties between the radically-initiated resin and base-catalyzed resin is attributed to the difference in the mechanism of network formation. Radical polymerizations of thiol-acrylate systems are known to afford inhomogeneous networks in which the cross-links are unevenly distributed.[42] In contrast, the base-catalyzed resin is formed *via* a step-growth mechanism where the distance between cross-links is determined by the polymer chains' length theoretically leading to a more homogenous network. Thermomechanical experiments could provide insight into the network topologies, however, the PBG materials were too soft to be analyzed. Differential scanning calorimetry did provide the glass transition temperature (Fig. S10†) which was around −55 °C for both networks. Interestingly, our gel fraction experiments (Tables S2–4†) determined that the degree of conversion for the radical and base-catalyzed reactions afforded similar extents of polymerization, but FTIR of the pucks show the presence of residual thiols in the radically cured gel (Fig. S12†). The differences between the two polymer networks could arise from the network topology and crosslinking density.[43]

Rheological analysis of the cured ionogels provided additional information on the crosslinking density of the material. Amplitude sweeps were used to identify the linear viscoelastic region (LVR) of each ionogel. The experiments showed that the radical initiated sample yielded at 2.5% strain and the PBG cured sample yielded at 16% strain (Fig. S7†) confirming that the radical samples are less ductile. Frequency sweeps in the LVR of the ionogels showed that the plateau modulus of the radical resin was higher than that of the PBG resin. As shown in eqn (2), the plateau storage modulus (G'_∞) is proportional to the crosslinking density (υ)

$$G'_\infty = \upsilon k_B T \quad (2)$$

where T is temperature and K_B is the Boltzmann constant. Therefore, conducting frequency sweeps in the linear viscoelastic region of the material will provide us with G'_∞ . Frequency sweeps were performed on 8 mm diameter by 1 mm thick cylinders of the cured gels (Fig. 4d). The results showed that the radical-mediated gel has a higher storage modulus, and therefore a higher degree of crosslinking density than the gels cured *via* a base-catalyzed pathway. Given that acrylates

Table 1 Summary of the dimensional accuracy of the optimization chip's channels and features (lines between channels)

Expected channel width [μm]	Observed channel width [μm]	Ratio obs : exp	Expected feature width [μm]	Observed feature width [μm]	Ratio obs : exp
1000	729.64 ± 37.28	0.73	500	663.24 ± 14.63	1.33
500	311.24 ± 53.91	0.62	500	610.12 ± 4.64	1.22
250	144.75 ± 29.97	0.58	250	344.22 ± 47.02	1.38
100	0	0	100	0	0

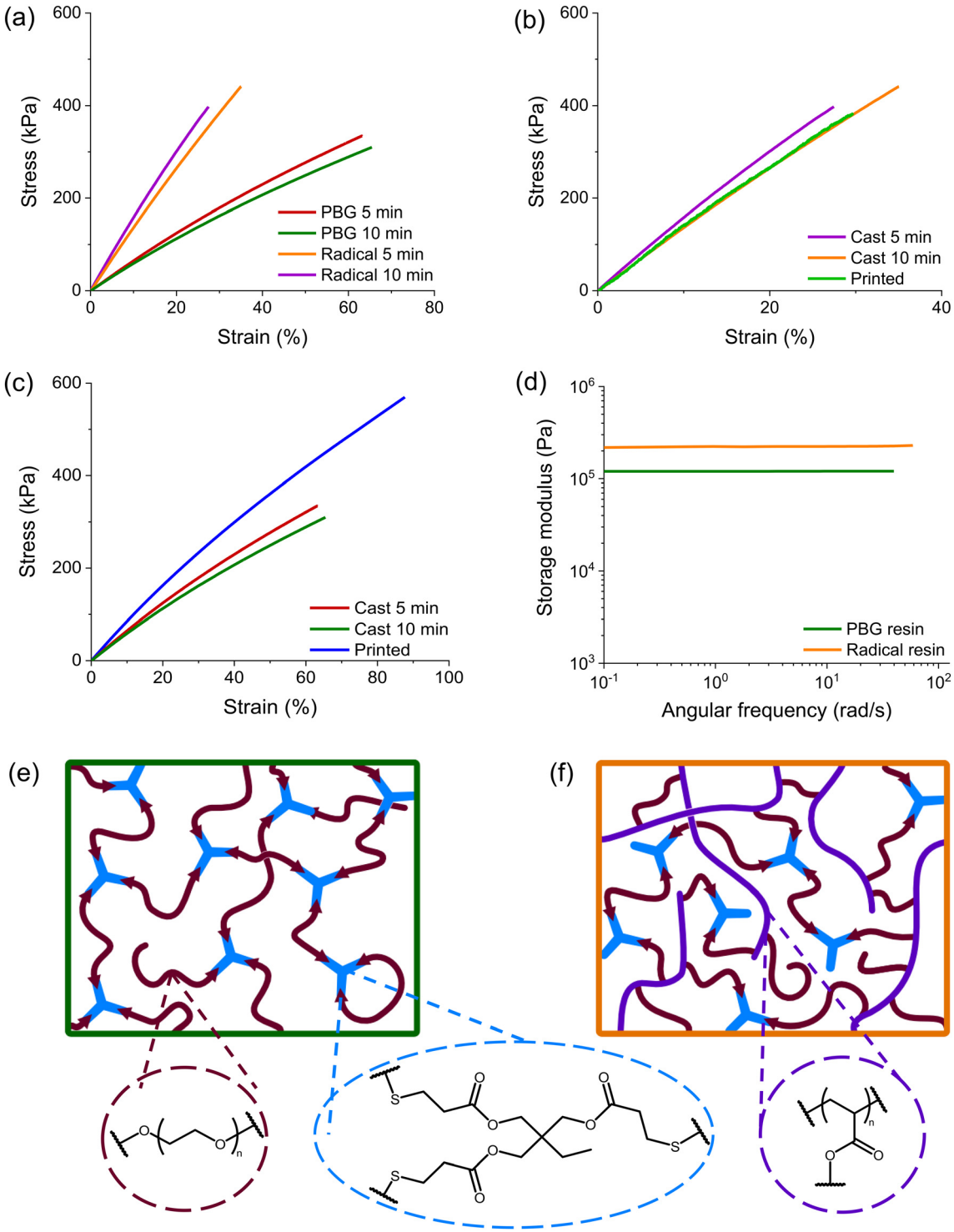

Fig. 4 Mechanical properties comparing radical and PBG resins. (a) tensile experiments comparing cast dogbones of radical-mediated resin to base-catalyzed resin. (b) Comparing printed *vs.* cast dogbones of radical-mediated resin. (c) Comparing printed *vs.* cast dogbones of base-catalyzed resin. (d) Frequency sweeps comparing the gels made with radical and PBG resins. Schematic representations of (e) the base-catalyzed network and (f) the radical-mediated network.

homopolymerize at faster rates than radical thiol-ene[34] monomers, we hypothesize that the higher crosslinking density is a result of polyacrylate forming (Fig. 4f, purple lines). This higher degree of crosslinking results in the material having less ductility as well. Although the PBG resin had less crosslinking density (Fig. 4e), the small molecular weight PEG used

likely still led to a crosslinking density that was too high to allow for the exchange of the thiol-Michael bonds indicative by the absence of stress relaxation in the material (Fig. S13†).[44] The thiol-Michael bond exchange requires good chain mobility to allow diffusion of reactive groups and produce relaxation or self-healing which in a highly crosslinked network is unlikely.[45]

Lastly, ionic liquids are innately ionically conductive because the salt pair is capable of self-diffusing and have excellent thermally stability.[30,46] When this salt pair is confined into a polymer matrix, the resulting ionogel will be stable in ambient conditions and ionically conductive while the polymer network provides mechanical stability. Electrical impedance spectroscopy (EIS) measurements are one method to determine ionic conductivity. These measurements were performed on printed discs and carried out on an Autolab 302N potentiostat galvanostat (Fig. S14†) and the results demonstrated that the material is ionically conductive as a printed gel with conductivity values ranging from 0.871 mS cm^{-1} to 69.7 μS cm^{-1} at 100 °C to 30 °C, respectively. These values are comparable to our previously published where we have used the conductivity for pressure sensors[25,26,47] and for mechano-activation.[27,48] Thermal properties were collected showing that the gel had excellent thermal stability (Fig. S11†) with degradation of the polymer occurring at 360 °C and ionic liquid degrading at 450 °C.

3. Conclusions

In conclusion, we formulated a 3D printable ionogel resin using a thiol-Michael polymerization for network formation. The photobase generator, NPPOC-TMG, was effective in catalyzing the thiol-Michael step-growth polymerization allowing for the printing of micro-featured structures within a reasonable time on a commercial DLP printer. The ionic liquid aided in the dissolution of tetraphenylborate PBG, decreased the gel point of the NPPOC-TMG resin, and provided ionic conductivity to the printed parts. The stability and UV curing behavior of the resin along with the mechanical and conductive properties of the material were studied. We found that the base-catalyzed thiol-Michael resin resulted in more ductile materials when compared to radical-mediated resin. This study showed an alternative method to incorporate PBG into vat photopolymerization using ionic liquids which provide added functionality to printed structures. Future studies will focus on resin optimization with photoabsorbers to improve the resolution of the prints and the application of these ionogel resins toward piezoionic sensors.

Author contributions

A. V., X. L. P., N. B., H. S., and A. N. conceived the project and designed the experiments. A. N. and H. S. oversaw the project. X. L. P. collected EIS and stress-relaxation data. N. S. aided in tensile experiments and rheology experiments. A. S. collected Keyence Microscope images. A. V. and A. N. wrote the manuscript, with contributions from all authors. All authors have given approval to the final version of the manuscript.

Data availability

The data supporting this article have been included as part of the ESI.†

Conflicts of interest

The authors declare no conflict of interest.

Acknowledgements

Part of this work was supported by the United States National Science Foundation (NSF) Emerging Frontiers in Research and Innovation award 2223537. A. V. gratefully acknowledges the support provided by the state of Washington through the University of Washington Clean Energy Institute and the Seattle branch of the ARCS foundation. The authors acknowledge the use of facilities and instrumentation (NMR) supported by the U.S. National Institutes of Health (NIH S10 OD030224-01A1). X. L. P gratefully acknowledges the support from the Spanish Ministry of Universities (FPU18/04904) and (EST23/00302).

References

1 A. Jandyal, I. Chaturvedi, I. Wazir, A. Raina and M. I. Ul Haq, 3D Printing – A Review of Processes, Materials and Applications in Industry 4.0, *Sustain. Oper. Comput.*, 2022, **3**, 33–42, DOI: **10.1016/j.susoc.2021.09.004**.

2 B. E. Kelly, I. Bhattacharya, H. Heidari, M. Shusteff, C. M. Spadaccini and H. K. Taylor, Volumetric Additive Manufacturing via Tomographic Reconstruction, *Science*, 2019, **363**(6431), 1075–1079, DOI: **10.1126/science.aau7114**.

3 B. J. Lee, K. Hsiao, G. Lipkowitz, T. Samuelsen, L. Tate and J. M. DeSimone, Characterization of a 30 Mm Pixel Size CLIP-Based 3D Printer and Its Enhancement through Dynamic Printing Optimization, *Addit. Manuf.*, 2022, **55**, 102800, DOI: **10.1016/j.addma.2022.102800**.

4 F. Zhang, L. Zhu, Z. Li, S. Wang, J. Shi, W. Tang, N. Li and J. Yang, The Recent Development of Vat Photopolymerization: A Review, *Addit. Manuf.*, 2021, **48**, 102423, DOI: **10.1016/j.addma.2021.102423**.

5 A. Bagheri and J. Jin, Photopolymerization in 3D Printing, *ACS Appl. Polym. Mater.*, 2019, **1**(4), 593–611, DOI: **10.1021/acsapm.8b00165**.

6 P. Marx, A. Romano, I. Roppolo, A. Chemelli, I. Mühlbacher, W. Kern, S. Chaudhary, T. Andritsch, M. Sangermano and F. Wiesbrock, 3D-Printing of High-κ

Thiol-Ene Resins with Spiro-Orthoesters as Anti-Shrinkage Additive, *Macromol. Mater. Eng.*, 2019, **304**(12), 1900515, DOI: 10.1002/mame.201900515.

7 L. Shahzadi, F. Maya, M. C. Breadmore and S. C. Thickett, Functional Materials for DLP-SLA 3D Printing Using Thiol–Acrylate Chemistry: Resin Design and Postprint Applications, *ACS Appl. Polym. Mater.*, 2022, **4**(5), 3896–3907, DOI: 10.1021/acsapm.2c00358.

8 E. Rossegger, Y. Li, H. Frommwald and S. Schlögl, Vat Photopolymerization 3D Printing with Light-Responsive Thiol-Norbornene Photopolymers, *Monatsh. fur Chem.*, 2023, **154**(5), 473–480, DOI: 10.1007/s00706-022-03016-5.

9 P. Lu, D. Ahn, R. Yunis, L. Delafresnaye, N. Corrigan, C. Boyer, C. Barner-Kowollik and Z. A. Page, Wavelength-Selective Light-Matter Interactions in Polymer Science, *Matter*, 2021, **4**(7), 2172–2229, DOI: 10.1016/j.matt.2021.03.021.

10 E. Blasco, M. Wegener and C. Barner-Kowollik, Photochemically Driven Polymeric Network Formation: Synthesis and Applications, *Adv. Mater.*, 2017, **29 (15)**, 1604005, DOI: 10.1002/adma.201604005.

11 N. Zivic, P. K. Kuroishi, F. Dumur, D. Gigmes, A. P. Dove and H. Sardon, Recent Advances and Challenges in the Design of Organic Photoacid and Photobase Generators for Polymerizations, *Angew. Chem., Int. Ed.*, 2019, **58**(31), 10410–10422, DOI: 10.1002/anie.201810118.

12 S. Honda, Organocatalytic Vat-Ring-Opening Photopolymerization Enables 3D Printing of Fully Degradable Polymers, *Commun. Chem.*, 2023, **6**(1), 1–4, DOI: 10.1038/s42004-023-00985-4.

13 K.-Y. Chung, A. Uddin and Z. A. Page, Record Release of Tetramethylguanidine Using a Green Light Activated Photocage for Rapid Synthesis of Soft Materials, *Chem. Sci.*, 2023, **14**(39), 10736–10743, DOI: 10.1039/D3SC04130A.

14 M. T. Kiker, A. Uddin, L. M. Stevens, K.-Y. Chung, P. Lu and Z. A. Page, Visible Light Activated Coumarin Photocages: An Interplay between Radical and Organobase Generation to Govern Thiol–Ene Polymerizations, *Polym. Chem.*, 2023, **14**(33), 3843–3850, DOI: 10.1039/D3PY00771E.

15 Z. Geng, J. J. Shin, Y. Xi and C. J. Hawker, Click Chemistry Strategies for the Accelerated Synthesis of Functional Macromolecules, *J. Polym. Sci.*, 2021, **59 (11)**, 963–1042, DOI: 10.1002/pol.20210126.

16 X. Zhang, W. Xi, G. Gao, X. Wang, J. W. Stansbury and C. N. Bowman, *O* -Nitrobenzyl-Based Photobase Generators: Efficient Photoinitiators for Visible-Light Induced Thiol-Michael Addition Photopolymerization, *ACS Macro Lett.*, 2018, **7**(7), 852–857, DOI: 10.1021/acsmacrolett.8b00435.

17 X. Zhang, W. Xi, S. Huang, K. Long and C. N. Bowman, Wavelength-Selective Sequential Polymer Network Formation Controlled with a Two-Color Responsive Initiation System, *Macromolecules*, 2017, **50**(15), 5652–5660, DOI: 10.1021/acs.macromol.7b01117.

18 D. P. Nair, M. Podgórski, S. Chatani, T. Gong, W. Xi, C. R. Fenoli and C. N. Bowman, The Thiol-Michael Addition Click Reaction: A Powerful and Widely Used Tool in Materials Chemistry, *Chem. Mater.*, 2014, **26**(1), 724–744, DOI: 10.1021/cm402180t.

19 D. R. Berry, B. K. Díaz, A. Durand-Silva and R. A. Smaldone, Radical Free Crosslinking of Direct-Write 3D Printed Hydrogels through a Base Catalyzed Thiol-Michael Reaction, *Polym. Chem.*, 2019, **10**(44), 5979–5984, DOI: 10.1039/C9PY00953A.

20 X. Lopez de Pariza, O. Varela, S. O. Catt, T. E. Long, E. Blasco and H. Sardon, Recyclable Photoresins for Light-Mediated Additive Manufacturing towards Loop 3D Printing, *Nat. Commun.*, 2023, **14**(1), 5504, DOI: 10.1038/s41467-023-41267-w.

21 M. T. Kiker, A. Uddin, L. M. Stevens, C. J. O'Dea, K. S. Mason and Z. A. Page, Onium Photocages for Visible-Light-Activated Poly(Thiourethane) Synthesis and 3D Printing, *J. Am. Chem. Soc.*, 2024, **146**(29), 19704–19709, DOI: 10.1021/jacs.4c07220.

22 M. T. Kiker, E. A. Recker, A. Uddin and Z. A. Page, Simultaneous Color- and Dose-Controlled Thiol–Ene Resins for Multimodulus 3D Printing with Programmable Interfacial Gradients, *Adv. Mater.*, 2024, **36**(40), 2409811, DOI: 10.1002/adma.202409811.

23 M. P. Jeske, M. J. Bonino, X. Huang, D. R. Harding, Y. Lu and M. Anthamatten, Two-Photon Printing of Base-Catalyzed Resins Involving Thiol-Michael Network Formation, *Adv. Mater. Technol.*, 2024, **9**, 2400100, DOI: 10.1002/admt.202400100.

24 J. Odent, T. J. Wallin, W. Pan, K. Kruemplestaedter, R. F. Shepherd and E. P. Giannelis, Highly Elastic, Transparent, and Conductive 3D-Printed Ionic Composite Hydrogels, *Adv. Funct. Mater.*, 2017, **27**(33), 1701807, DOI: 10.1002/adfm.201701807.

25 B. Narupai, J. Wong, E. Sanchez-Rexach, J. Smith-Jones, V. C. T. Le, N. Sadaba, H. Sardon and A. Nelson, 3D Printing of Ionic Liquid Polymer Networks for Stretchable Conductive Sensors, *Adv. Mater. Technol.*, 2023, **8**, 2300226, DOI: 10.1002/admt.202300226.

26 J. Wong, A. T. Gong, P. A. Defnet, L. Meabe, B. Beauchamp, R. M. Sweet, H. Sardon, C. L. Cobb and A. Nelson, 3D Printing Ionogel Auxetic Frameworks for Stretchable Sensors, *Adv. Mater. Technol.*, 2019, **4**(9), 1900452, DOI: 10.1002/admt.201900452.

27 J. Wong, A. Basu, M. Wende, N. Boechler and A. Nelson, Mechano-Activated Objects with Multidirectional Shape Morphing Programmed via 3D Printing, *ACS Appl. Polym. Mater.*, 2020, **2**(7), 2504–2508, DOI: 10.1021/acsapm.0c00588.

28 K. Lee, Y. Shang, V. A. Bobrin, R. Kuchel, D. Kundu, N. Corrigan and C. Boyer, 3D Printing Nanostructured Solid Polymer Electrolytes with High Modulus and Conductivity, *Adv. Mater.*, 2022, **34**(42), 2204816, DOI: 10.1002/adma.202204816.

29 D. Melodia, A. Bhadra, K. Lee, R. Kuchel, D. Kundu, N. Corrigan and C. Boyer, 3D Printed Solid Polymer Electrolytes with Bicontinuous Nanoscopic Domains for

Ionic Liquid Conduction and Energy Storage, *Small*, 2023, **19**(50), 2206639, DOI: **10.1002/smll.202206639**.

30 L. Bideau, J. Viau, L. Vioux and A. Ionogels, Ionic Liquid Based Hybrid Materials, *Chem. Soc. Rev.*, 2011, **40**(2), 907–925, DOI: **10.1039/C0CS00059K**.

31 R. J. Mondschein, A. Kanitkar, C. B. Williams, S. S. Verbridge and T. E. Long, Polymer Structure-Property Requirements for Stereolithographic 3D Printing of Soft Tissue Engineering Scaffolds, *Biomaterials*, 2017, **140**, 170–188, DOI: **10.1016/j.biomaterials.2017.06.005**.

32 B. D. Mather, K. Viswanathan, K. M. Miller and T. E. Long, Michael Addition Reactions in Macromolecular Design for Emerging Technologies, *Prog. Polym. Sci.*, 2006, **31**(5), 487–531, DOI: **10.1016/j.progpolymsci.2006.03.001**.

33 G. A. Appuhamillage, N. Chartrain, V. Meenakshisundaram, K. D. Feller, C. B. Williams and T. E. Long, 110th Anniversary: Vat Photopolymerization-Based Additive Manufacturing: Current Trends and Future Directions in Materials Design, *Ind. Eng. Chem. Res.*, 2019, **58**(33), 15109–15118, DOI: **10.1021/acs.iecr.9b02679**.

34 S. Chatani, T. Gong, B. A. Earle, M. Podgórski and C. N. Bowman, Visible-Light Initiated Thiol-Michael Addition Photopolymerization Reactions, *ACS Macro Lett.*, 2014, **3**(4), 315–318, DOI: **10.1021/mz500132j**.

35 P. F. Jacobs, *Fundamentals of Stereolithography*, 1992.

36 D. A. Rau, J. P. Reynolds, J. S. Bryant, M. J. Bortner and C. B. Williams, A Rheological Approach for Measuring Cure Depth of Filled and Unfilled Photopolymers at Additive Manufacturing Relevant Length Scales, *Addit. Manuf.*, 2022, **60**, 103207, DOI: **10.1016/j.addma.2022.103207**.

37 T. J. Kolibaba, J. P. Killgore, B. W. Caplins, C. I. Higgins, U. Arp, C. C. Miller, D. L. Poster, Y. Zong, S. Broce, T. Wang, V. Talačka, J. Andersson, A. Davenport, M. A. Panzer, J. R. Tumbleston, J. M. Gonzalez, J. Huffstetler, B. R. Lund, K. Billerbeck, A. M. Clay, M. R. Fratarcangeli, H. J. Qi, D. H. Porcincula, L. B. Bezek, K. Kikuta, M. N. Pearlson, D. A. Walker, C. J. Long, E. Hasa, A. Aguirre-Soto, A. Celis-Guzman, D. E. Backman, R. L. Sridhar, K. A. Cavicchi, R. Viereckl, E. Tong, C. J. Hansen, D. M. Shah, C. Kinane, A. Pena-Francesch, C. Antonini, R. Chaudhary, G. Muraca, Y. Bensouda, Y. Zhang and X. Zhao, Results of an Interlaboratory Study on the Working Curve in Vat Photopolymerization, *Addit. Manuf.*, 2024, **84**, 104082, DOI: **10.1016/j.addma.2024.104082**.

38 K. M. Leong, A. Y. Sun, M. L. Quach, C. H. Lin, C. A. Craig, F. Guo, T. R. Robinson, M. M. Chang and A. O. Olanrewaju, Democratizing Access to Microfluidics: Rapid Prototyping of Open Microchannels with Low-Cost LCD 3D Printers, *ACS Omega*, 2023, **9**, 45537–45544, DOI: **10.1021/acsomega.4c07776**.

39 D. Karis and A. Nelson, Time-Dependent Covalent Network Formation in Extrudable Hydrogels, *Polym. Chem.*, 2020, **11**(43), 6910–6918, DOI: **10.1039/D0PY01129K**.

40 J. M. Sirrine, V. Meenakshisundaram, N. G. Moon, P. J. Scott, R. J. Mondschein, T. F. Weiseman, C. B. Williams and T. E. Long, Functional Siloxanes with Photo-Activated, Simultaneous Chain Extension and Crosslinking for Lithography-Based 3D Printing, *Polymer*, 2018, **152**, 25–34, DOI: **10.1016/j.polymer.2018.02.056**.

41 P. J. Scott, V. Meenakshisundaram, N. A. Chartrain, J. M. Sirrine, C. B. Williams and T. E. Long, Additive Manufacturing of Hydrocarbon Elastomers via Simultaneous Chain Extension and Cross-Linking of Hydrogenated Polybutadiene, *ACS Appl. Polym. Mater.*, 2019, **1**(4), 684–690, DOI: **10.1021/acsapm.8b00150**.

42 Q. Thijssen, L. Parmentier, E. Augustyniak, P. Mouthuy, V. Vlierberghe and S. From, Chain Growth to Step Growth Polymerization of Photoreactive Poly–ε–Caprolactone: The Network Topology of Bioresorbable Networks as Tool in Tissue Engineering, *Adv. Funct. Mater.*, 2022, **32**(20), 2108869, DOI: **10.1002/adfm.202108869**.

43 Y. Gu, J. Zhao and J. A. Johnson, Polymer Networks: From Plastics and Gels to Porous Frameworks, *Angew. Chem., Int. Ed.*, 2020, **59**(13), 5022–5049, DOI: **10.1002/anie.201902900**.

44 B. Shi and M. F. Greaney, Reversible Michael Addition of Thiols as a New Tool for Dynamic Combinatorial Chemistry, *Chem. Commun.*, 2005, **7**, 886–888, DOI: **10.1039/B414300K**.

45 B. Zhang, Z. A. Digby, J. A. Flum, P. Chakma, J. M. Saul, J. L. Sparks and D. Konkolewicz, Dynamic Thiol–Michael Chemistry for Thermoresponsive Rehealable and Malleable Networks, *Macromolecules*, 2016, **49 (18)**, 6871–6878, DOI: **10.1021/acs.macromol.6b01061**.

46 O. Zech, A. Stoppa, R. Buchner and W. Kunz, The Conductivity of Imidazolium-Based Ionic Liquids from (248 to 468) K. B. Variation of the Anion, *J. Chem. Eng. Data*, 2010, **55 (5)**, 1774–1778, DOI: **10.1021/je900793r**.

47 J. Smith-Jones, N. Ballinger, N. Sadaba, X. L. d. Pariza, Y. Yao, S. L. Craig, H. Sardon and A. Nelson, 3D Printed Modular Piezoionic Sensors Using Dynamic Covalent Bonds, *RSC Appl. Polym.*, 2024, **2**(3), 434–443, DOI: **10.1039/D3LP00289F**.

48 A. Basu, J. Wong, B. Cao, N. Boechler, A. J. Boydston and A. Nelson, Mechanoactivation of Color and Autonomous Shape Change in 3D-Printed Ionic Polymer Networks, *ACS Appl. Mater. Interfaces*, 2021, **13**(16), 19263–19270, DOI: **10.1021/acsami.1c01166**.